Int. J. Electrochem. Sci., 15 **(2020)** 8397 – 8407, doi: 10.20964/2020.09.44

International Journal of
ELECTROCHEMICAL
SCIENCE
www.electrochemsci.org

A Facile Strategy for Preparing Superhydrophobic Coating on AZ31 Magnesium Alloy with Stable Anticorrosion Performance

Shidong Wang[1,2], *Huifang Zhang*[1,2], *Zhiqiang Qian*[1,2], *Xiushen Ye*[1,2,*], *Zhijian Wu*[1,2,*], *Shengting Li*[3]

[1] Key Laboratory of Comprehensive and Highly Efficient Utilization of Salt Lake Resources, Qinghai Institute of Salt Lakes, Chinese Academy of Sciences, Xining 810008, China
[2] Key Laboratory of Salt Lake Resources Chemistry of Qinghai Province, Xining 810008, China
[3] Qinghai Salt Lake Industry Co., Ltd., Golmud 816099, China
[*]E-mail: yexs@isl.ac.cn, zjwu@isl.ac.cn

Received: 13 May 2020 / *Accepted:* 3 July 2020 / *Published:* 10 August 2020

Superhydrophobic coating on magnesium alloy by employing polydopamine@SiO_2 (PDA@SiO_2) particles and silane via a facile one-step spraying technique was prepared in this study. Surface morphology, chemical compositions, roughness and wettability of the coating were comprehensively investigated by Field Emission Scanning Electron Microscopy (FESEM), Fourier Transform Infrared Spectra (FTIR), 3D optical microscope and contact angle techniques, respectively. Corrosion resistance of the coating was evaluated by electrochemical impedance spectroscopy (EIS). Results indicated that the coating exhibited superhydrophobicity due to its micropapillae structure and low surface energy of silica aggregates. The coating showed outstanding superhydrophobicity with contact angle (CA) larger than 154° and sliding angle (SA) less than 3°. $|Z|_{0.01Hz}$ of superhydrophobic coated sample reached $6.916 \times 10^8\ \Omega \cdot cm^2$, which showed excellent corrosion performance. The superhydrophobic coating can protect the specimen surface from being eroded even after fifteen days immersion in NaCl solution, indicating that the coating had a strong stability in corrosive media.

Keywords: PDA@SiO_2, Superhydrophobic, Magnesium alloy, Anticorrosion

1. INTRODUCTION

Magnesium alloys have been used as lightweight structural materials for automobiles, aircrafts, electronic products, etc., owing to their low density, good consistency and high specific strength[1,2]. Due to the active chemical properties of magnesium and the inability to produce passivating films, magnesium alloys are prone to corrosion, which limits their applications in industry. To improve the corrosion resistance of magnesium alloys, various techniques have been investigated, such as chemical conversion[3,4], micro-arc oxidation[5,6], sol-gel coatings[7,8], etc. In recent years, the appearance of

superhydrophobic surface has provided a new idea for anticorrosion of magnesium alloys due to its unique hydrophobicity, which can reduce the direct contact from the substrate to the corrosive media.

The wettability of material surface mainly depends on the surface chemical properties and surface microstructure. Therefore, the hydrophobicity of the material surface is improved mainly by reducing the surface energy and increasing the surface roughness[9,10]. Up to now, numerous methods have been successfully developed to prepare superhydrophobic coatings on magnesium alloy, including electrochemical deposition[11,12], hydrothermal treatment[13,14], coating nanoparticles[15,16], and so on.

However, most techniques contained multiple steps via creating rough surfaces first and then modified with low surface energy materials, which were usually complicated and time-consuming. One-step approach was much more attractive because of their convenience, by which hierarchical structures and low surface energy can be simultaneously achieved. In this work, a simple and effective one-step nanoparticle spraying approach for constructing corrosion-resistant superhydrophobic surface over magnesium alloys was proposed.

2. EXPERIMENTAL

2.1. Materials

The AZ31 magnesium alloy sheets with the dimension of 60 mm × 40 mm × 3 mm were purchased from Dongguan Hongxing Metal Materials Co., Ltd. Tetraethoxysilane (TEOS, 98%), diethoxydimethylsilane (DEDMS, 97%), triethoxymethylsilane (MTES, 98%), 3-hydroxytyramine hydrochloride (DA, 98%), ammonium hydroxide solution ($NH_3 \cdot H_2O$, 25-28%), and ethanol (99.5%) were purchased from Shanghai Machlin Biochemical Co. Ltd. 1,1,1,3,3,3-hexamethyldisilazane (HMDS, 98%) was purchased from Shanghai Aladdin Bio-Chem Technology Co., Ltd. All chemicals were analytical grade reagents and were used as received.

2.2. Preparation of superhydrophobic SiO_2 nanoparticles

First, 12 mL of $NH_3 \cdot H_2O$ was mixed with 200 mL of ethanol and stirred for 10 min. Next, 16 mL of TEOS was added to the above mixture dropwisely and stirred for 5 h at room temperature. Subsequently, 0.12 g of DA was added into the solution while stirring. Then 32 mL HMDS was added drop by drop. After the hydrolysis reaction of 48 h, the brown HMDS-DA modified SiO_2 nanoparticles were collected through filtration and then dried in a vacuum oven at 80 ℃ for 2 h.

2.3. Superhydrophobic coating fabrication

The AZ31 magnesium alloy sheets were polished successively with 320, 800 and 1200 grit silicon carbide water abrasive sandpaper, and then washed in ethanol with ultrasonic cleaning for 5 min. The pieces were rinsed with deionized water and dried by hot air.

1 mL DEDMS and 1.5 mL MTES were ultrasonically dispersed in the mixture of ethanol (15 mL) and water (5 mL). The pH of the solution was then adjusted to about 4 with 100 μL acetic acid. Then 2.5g superhydrophobic SiO_2 nanoparticles were ultrasonically dispersed in the mixture. A homogeneous dispersion was formed after reaction of the mixture at 60 ℃ for 6 h under magnetic agitation. After the reaction completed, 4 mL of the mixture was uniformly sprayed onto the surface of the pretreated AZ31 magnesium alloy sheet with an airbrush (Infinity, Harder & Steenbeck, Germany) about 15 cm from the base at a N_2 pressure of 0.2 MPa. The magnesium alloy sheet was placed on an electric heating plate at 120℃ to accelerate ethanol volatilization during spraying. Finally, the sample was dried in a 100℃ oven for 1 h to obtain the superhydrophobic coating. The schematic diagram of fabrication process of superhydrophobic coating was shown in Fig. 1.

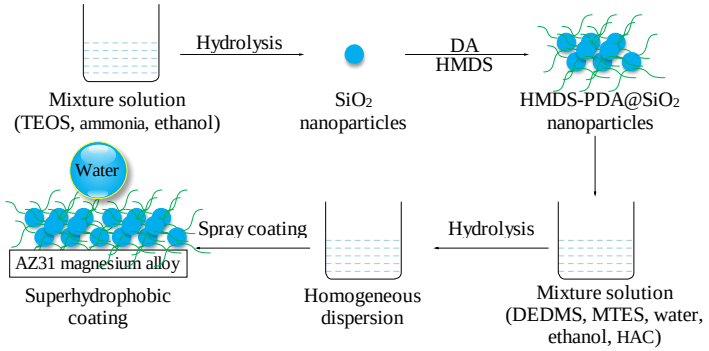

Figure 1. Schematic diagram of fabrication process of superhydrophobic coating.

2.4. Characterization and tests

The surface morphology of the sample was observed using a Hitachi SU8010 FESEM. The chemical composition of the sample surface was analyzed by the Fourier transform infrared spectrometer (Nexus, Thermo Nicollet, USA). The counter image and three-dimensional images of the surface were analyzed by a 3D optical microscope (ContourGT-X, Bruker). The static contact angles and sliding angles of water droplet were characterized by an optical contact angle measuring instrument (DSA25, Kruss, Germany). The droplet volume was measured at 5 μL. The profile of free droplet on the superhydrophobic coating was monitored by a video camera connected to a computer. All the measurements were averaged at 5 different points of the sample.

The electrochemical measurements were performed in 3.5 wt% NaCl solution by electrochemical workstation (PGSTAT 128N) to evaluate the corrosion resistance of the coating. In the measurements, a three-electrode system was used, with magnesium alloy sheet as the working electrode, a platinum sheet as the auxiliary electrode, a saturated calomel electrode (SCE) as the reference electrode, and the exposed area of the sample was $1cm^2$.EIS were measured in the frequency range from 10^5 Hz to 10^{-2} Hz with the perturbation potential of 10 mV at the open circuit potential. The EIS spectra were fitted using the ZSimpWin software. To confirm the reliability of the electrochemical parameters, the electrochemical experiments were repeated three times.

3. RESULTS AND DISCUSSION

3.1. Structure and characterization of superhydrophobic SiO_2 nanoparticles and coating

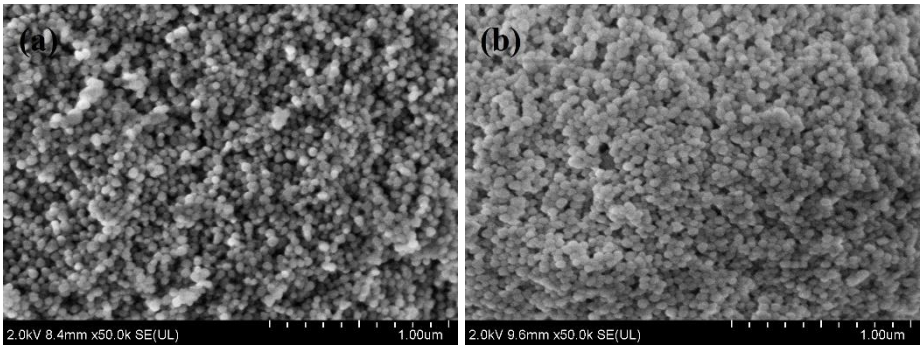

Figure 2. SEM images of (a) modified SiO_2 nanoparticles and (b) coating.

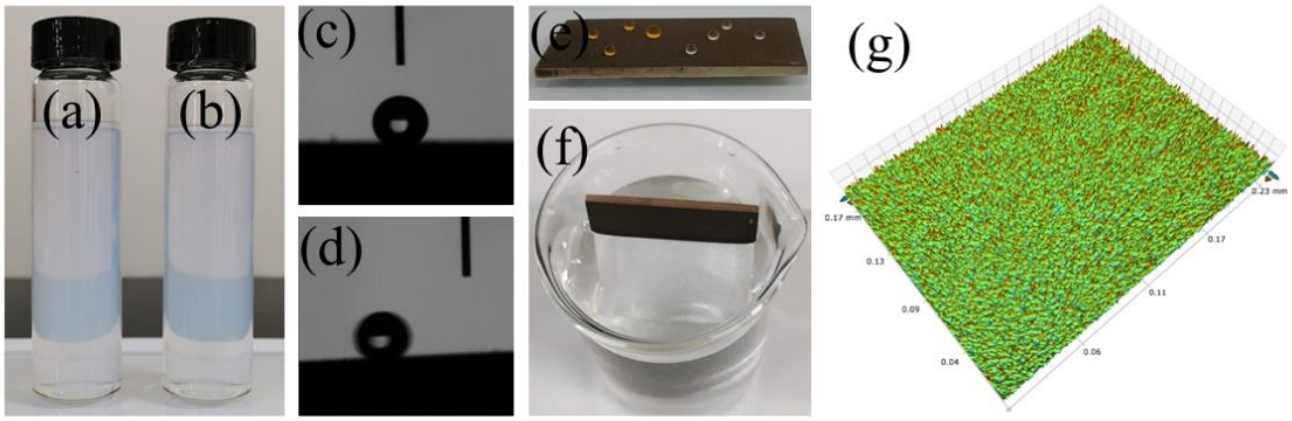

Figure 3. Optical images of (a) SiO_2 suspension modified without dopamine before centrifugation and (b) after centrifugation, measurements of (c) CA and (d) SA, (e) droplets of methyl orange solution and water on coated magnesium alloy, (f) coated magnesium alloy immersed in deionized water. (g) 3D topography of superhydrophobic coating.

The micro/nano structure and morphologies of superhydrophobic SiO_2 nanoparticles and coating were shown in Fig.2. It was clearly shown that the diameter of nanoparticles was about 40nm. First, SiO_2 nanoparticles were obtained through Stober process. Then the nanoparticles were modified by HMDS-DA. Inspired by high adhesion ability of marine mussels, in situ spontaneous polymerization of DA can effectively modify the surface of any material. More importantly, PDA is rich in catechol and amine groups, which can be used as a platform for further modification, including the immobilization of nanoparticles, chemical reactions, etc., and is widely used in the preparation of superhydrophobic materials[17-24]. In the experiment, DA can be transformed into PDA as it can be oxidized and spontaneously self-polymerized under alkaline conditions with oxygen as the oxidant. Through the sol-gel process, the silica precursor TEOS hydrolyzed and interacted with the active groups on the PDA surface, which led to cross-linked structures and strong covalent and noncovalent interactions with silica were formed. The PDA provided bridges to making silica nanoparticles connect with each other and

promoted the formation of aggregation. Two important functions were served by PDA, one as a bond between silica nanoparticles, and the other as an active substrate. When DA was not added in the modification process, silica suspension was stable that could not be centrifuged as shown in Fig. 3. (a, b). Due to the presence of HMDS in the system, the –OH groups on the surface of SiO_2 were converted. The high hydrophobicity of $–CH_3$ groups provided low surface energy for nanoparticles[18].

The coating was stacked by the modified particles homogenously coated by DEDMS-MTES sol matrix and a micro/nano-scale roughness was formed by nanoparticle aggregates displayed in Fig.1b. The coating showed outstanding superhydrophobicity with CA larger than 154º and SA less than 3º, as shown in Fig. 3 (c, d). The optical photograph of wettability performance of droplets of methyl orange solution and water on coated magnesium alloy was shown in Fig. 3e, excellent liquid-repellency can be more directly reflected by the nearly spherical state of many randomly distributed liquids on the surface. The cluster morphology formed by silica aggregates was beneficial to form micropapillae structure for improving surface roughness. These rough structures could capture air to form air film on the surface of the coating. Fig. 3f showed the surface of superhydrophobic coated magnesium alloy immersed in deionized water. Compared to the brown coating, the surface under water showed silver white, which was caused by the reflection of light from the air layer on the surface of the superhydrophobic coating[25-27]. In order to further characterize the roughness of the prepared superhydrophobic coating, 3D optical microscope was used to evaluate the surface roughness. Fig. 3g showed 3D topography of the superhydrophobic coating, a rough structure (Ra = 1.293 μm) can be observed. The panoramic morphology of the sample indicated uniformly distributed protuberance surface. These results indicated that superhydrophobic coating was successfully obtained on magnesium alloy.

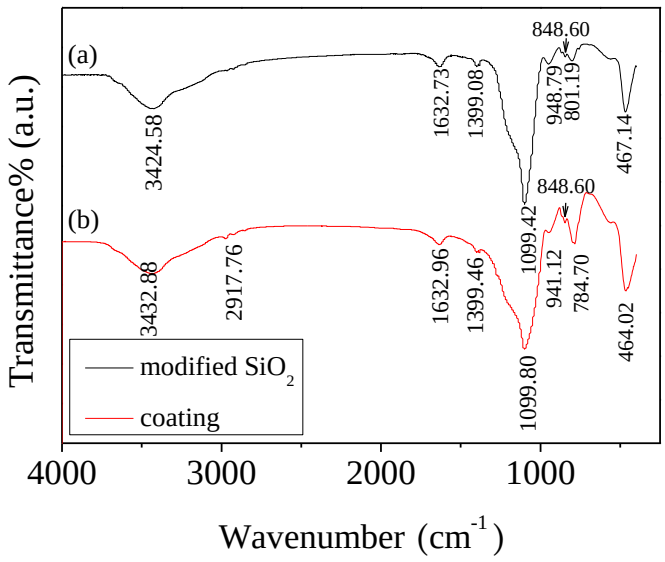

Figure 4. FTIR spectra of (a) modified SiO_2 particles (b) superhydrophobic coating.

The wetting behavior of surfaces was not only controlled by surface morphologies but also controlled by chemical composition of the surface. The chemical compositions of the modified SiO_2

nanoparticles and coating on magnesium alloy were investigated by FTIR spectroscopy. As shown in Fig. 4, all characteristic absorption peaks were observed in the range of 400-4000 cm^{-1}.

For modified SiO_2 nanoparticles, the broad peak located at 3423 cm^{-1} attributed to phenolic OH and NH groups[28,29]. The absorption bands at 1632.73 cm^{-1} corresponded to characteristic stretching vibration of C=C bonds[17]. The small peaks at 1399.08 cm^{-1} indicated vibration absorption of C–N bonds. These characterization results indicated the successful synthesis of PDA. The absorption bands at 1099.42 cm^{-1} indicated the bending vibrations of Si–O–Si bonds[24,30]. The absorption bands at 948.79 and 801.19 cm^{-1} corresponded to stretching vibrations of Si–O–Si bonds[31]. Small peaks at 848.60 cm^{-1} corresponded to characteristic –Si(CH_3) stretching vibrations[31]. The adsorption peak at 467.14 cm^{-1} can be attributed to the presence of Si–OH bonds[31]. These observations demonstrated that silica had been successfully modified by HMDS. The FTIR spectra of the coating was similar to modified SiO_2 particles. A new strong band at 784.70 cm^{-1} corresponded to –Si(CH_3) stretching vibrations. The peak ascribed to C–H stretching in the –CH_3 at 2917.76 cm^{-1} became stronger[32,33]. They suggested that MTES and DEDMS successfully packaged on the SiO_2 particles.

3.2 Corrosion resistance of superhydrophobic coating

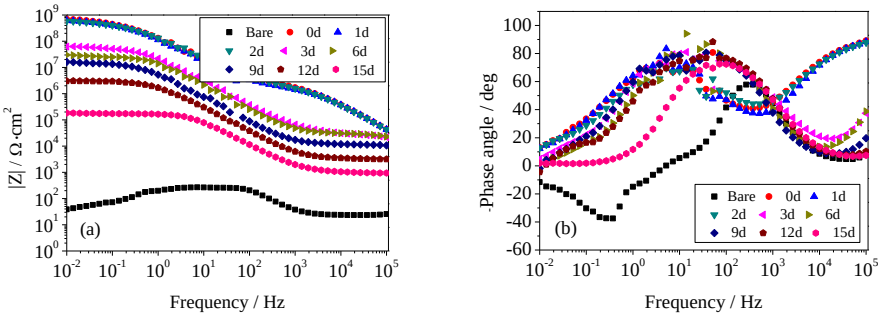

Figure 5. Bode-|Z| (a) and Bode-phase angle (b) versus frequency plots of bare AZ31 and superhydrophobic coated sample immersed in 3.5wt% NaCl solution.

In this work, 3.5wt% NaCl solution was used as corrosive solution. EIS obtained from electrochemical experiments were used to evaluate corrosion resistance of superhydrophobic coating. The Bode diagrams of bare AZ31 and superhydrophobic coated sample immersed in 3.5wt% NaCl solution were shown in Fig.5. In Bode plots, the impedance modulus at the low-frequency zone was in connection with the corrosion resistance of the coating. It was well known that the higher the low-frequency Z modulus usually resulted in better anticorrosion performance. The impedance modulus of bare AZ31 was around 260 $\Omega \cdot cm^2$ (10 Hz), and presented a decline trend after this highest value with a positive phase shift at the same time, which showed the inductive behavior of bare AZ31, and this inductive behavior indicated the poor corrosion resistance[34]. As seen from the Fig.3, $|Z|_{0.01Hz}$ of superhydrophobic coated sample reached $6.916 \times 10^8 \Omega \cdot cm^2$. It was well accepted that larger impedance modulus at the low-frequency domain was an indication of better corrosion protection performance because the vulnerable metal substrate was separated by the coating layer from corrosive species. During

immersion process, EIS was used to monitor the remaining corrosion inhibition of the coating. The impedance modulus of the sample decreased over the immersion period, indicating the decrease of the corrosion resistance with the immersion time.

The phase angle curve of bare AZ31 showed one time constant in the middle frequency region and one time constant in the low frequency region which was in relation to the corrosion process. For the superhydrophobic coated sample, there were two time constant can be seen from the curves: one time constant was in the middle frequency region and the other one was at high frequencies reached approximately 90°, which proved the presence of an outer layer[35]. As the immersion time lengthened, the phase angle at high frequencies decreased, which indicated the degradation of protective performance of the outer layer[36]. With the immersion time lengthened to three days, the phase angle at high frequencies suddenly decreased to 37.48°, indicating the outer layer of the coating was soaked. With the extension of immersion time, the phase angle decreased slowly, and when the immersion reached fifteen days, the phase angle dropped to 7.47°.

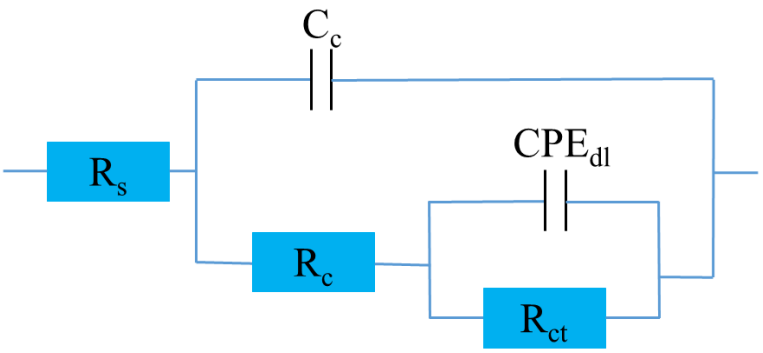

Figure 6. The equivalent circuit of superhydrophobic coated sample immersed in 3.5wt% NaCl solution.

Table 1. EIS fitting parameters for superhydrophobic coated sample.

Immersion time (d)	C_c (F·cm^{-2})	R_c (Ω·cm^2)	CPE_{dl} (F·cm^{-2})	R_{ct} (Ω·cm^2)
0	3.996E-11	1.978E6	1.737E-9	7.102E8
1	3.963E-11	1.593E6	1.903E-9	6.184E8
2	4.023E-11	1.549E6	1.795E-9	6.069E8
3	7.675E-11	2.475E4	8.571E-9	6.113E7
6	5.656E-11	2.758E4	1.093E-8	2.723E7
9	1.057E-10	8161	3.182E-8	1.5E7
12	8.626E-10	1137	8.411E-8	3.055E6
15	4.016E-8	508.8	2.253E-7	1.747E5

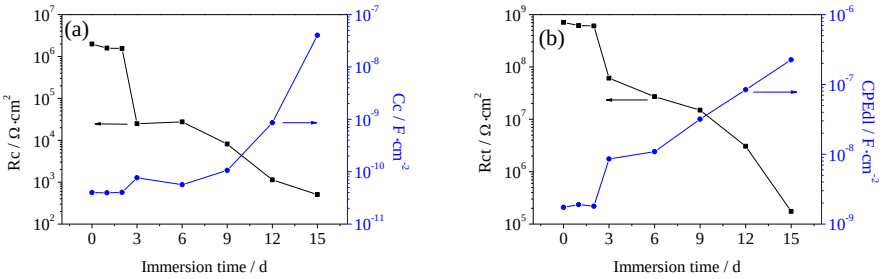

Figure 7. The evolution of capacitance and resistance upon immersion of membrane layer (a) and double electric layer (b) for superhydrophobic coated sample.

To further explore the electrochemical corrosion behavior of the sample precisely, the obtained experimental data were analyzed and understood via fitting the data using simple equivalent electrical circuit which was shown in Fig. 6. In the circuit, R_s is solution resistance, R_c and C_c are membrane resistance and capacitance, R_{ct} and CPE_{dl} are charge transfer resistance and constant phase element capacitance models of double electric layer. The fitting results were presented in Table 1. The evolution of capacitance and resistance upon immersion for superhydrophobic coated sample were shown in Fig. 7.

From Fig. 7a, with the extension of immersion time, R_c gradually decreased and C_c gradually increased, such behavior was considered as an indication of water uptake by the coating[37]. For the case of the superhydrophobic coating, it corresponded to partial penetration of the solution inside the surface texture with corresponding increase in the fraction of wetted area. It can be found that R_c value decreased sharply with the immersion time lengthened to three days, which had the same tendency as the phase angle at high frequencies. The outer layer of the coating was soaked by electrolyte solution and gradually lost its protective effect. Then the electrolyte solution gradually penetrated into the air cushion. The evolution of capacitance and resistance upon immersion of double electric layer presented in Fig. 6b had the same trend of membrane layer. At the first two days immersion, R_{ct} value changed slightly from $7.102 \times 10^8\,\Omega\cdot cm^2$ to $6.069 \times 10^8\,\Omega\cdot cm^2$. Due to the penetration of the electrolyte solution, R_{ct} value decreased to $6.113 \times 10^7\,\Omega\cdot cm^2$ sharply with the immersion time lengthened to three day. Then the R_{ct} value decreased slowly with the extension of immersion time. With increasing immersion time and water pressure, the corrosive media gradually squeezed into the pores of the microsized mastoids[38]. The increasing CPE_{dl} with immersion time can be ascribed to the diffusion of corrosive ions in the coating. As a result of gradually penetrating into superhydrophobic layer of Cl^-, that was to say the protection of the metal substrate was weakening little by little. Nevertheless, even after fifteen days immersion, R_{ct} value decreased to $1.747 \times 10^5\,\Omega\cdot cm^2$, suggested that the superhydrophobic layer can protect the specimen surfaces from being eroded. This indicated that the air cushion of the superhydrophobic coating was relatively stable and can effectively protect the metal substrate from corrosion. As a kind of biological adhesion substance, PDA provided a powerful interface for the formation of silica clusters. Durable multiscale surface roughness can be formed by closely-arranged silica clusters, keeping a stable air cushion in underwater conditions.

3.3 Anti-corrosion mechanisms

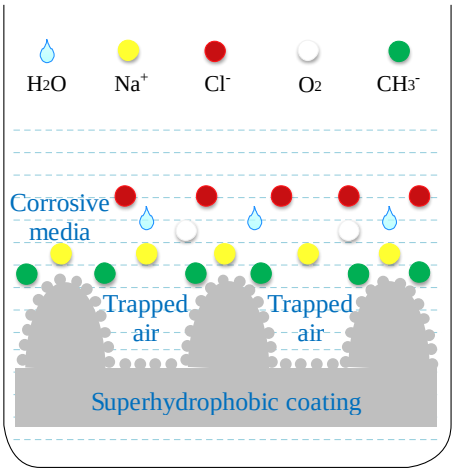

Figure 8. Schematic diagram of interface between superhydrophobic coating and NaCl solution.

According to the existing literature, the protective properties of the superhydrophobic coating on the metal surface are mainly derived from the repulsion of the superhydrophobic coating on the corrosive solution, inhibition of adsorption of corrosive ions, and the specific redistribution in the electric double layer of hydrophobic layers in solution[39-41].

Fig. 8 presented schematic diagram of interface between superhydrophobic coating and NaCl solution. Based on the air layer theory of Cassie-Baxter model and the capillary effect of its micro/nano structure, the multi-stage structure designed by PDA@SiO_2 on the surface of the coating had ability to store large amount of gas forming air cushion. When the superhydrophobic surface was immersed in the aqueous solution, the air layer was trapped in the micro/nano structure, forming a barrier between the metal matrix and the corrosive medium and inhibiting ion migration. In this study, the mirror effect as shown in Fig. 2f also confirmed the existence of an air layer. Only a very small portion of the coating surface was exposed to corrosive media, reducing the number of active corrosion sites. The air cushion between the superhydrophobic coating and the corrosive medium can effectively delayed the penetration of corrosive ions by blocking action.

In addition, the researchers found that corrosion protection of the superhydrophobic coating was not only related to the water repellency of the coating, but also to the physical and chemical properties of the interface between the coating and the corrosive medium[39-41]. The sol-gel system and silica particles contained a large number of hydrophobic groups $–CH_3$, which occupied the active corrosion sites on the coating and prevented the adsorption of corrosive ions and dissolved oxygen. The decrease of Cl^- adsorption on the hydrophobic layer inhibited the anode reaction, while the decrease of O_2 and H_2O adsorption inhibited the cathode reaction. In addition, in a neutral solution, the surfaces of various hydrophobic agents were negatively charged. The negative charge of hydrophobic groups caused the redistribution of the surface double layers and the decrease of the surface Cl^- concentration. Therefore, ordered hydrophobic groups acted as barriers to charge transfer.

With the extension of immersion time, some hydrophobic groups underwent hydrolysis and desorption from the coating interface, resulting in defects that were easily adsorbed by corrosive ions

Cl^-. At the same time, the dissolution process can lead to the removal of nanoparticles from the surface[42].

4. CONCLUSIONS

To summarize, a facile method was developed to achieve superhydrophobic coating on magnesium alloys with incorporating modified PDA@SiO_2 nanoparticles and DEDMS-MTES silanes. PDA connected silica nanoparticles to each other, promoting the formation of aggregates, facilitating the formation of micro-papillary structures and improving surface roughness. The corrosion resistance performance of the coating was studied by EIS measurement, and the results showed that the corrosion resistance of magnesium alloy can be effectively improved by the superhydrophobic coating. After immersion in NaCl solution for fifteen days, magnesium alloy can still be effectively prevented from corrosion, indicating that the coating had a strong stability in corrosive solution.

ACKNOWLEDGEMENTS
This work was financially supported by Qinghai Provincial Science and Technology Project (2018-ZJ-725), Hundred Talent Program of Haixi Mongolian and Tibetan Autonomous Prefecture.

References

1. M. Aparicio, J. Mosa1, G. Rodriguez, J. Guzman, Q. Picard, L.C. Klein, A. Jitianu, *ACS Appl. Mater. Interfaces*, 11 (2019) 3493.
2. T. Ishizaki, Y. Masuda, M. Sakamoto, *Langmuir*, 27 (2011) 4780.
3. K.H. Yang, M.D. Ger, W.H. Hwu, Y. Sung, Y.C. Liu, *Mater. Chem. Phys.*, 101 (2007) 480.
4. H. Zhang, R. Luo, W. Li, J. Wang, M.F. Maitz, J. Wang, G. Wan, Y. Chen, H. Sun, C. Jiang, R. Shen, N. Huang, *Corros. Sci.*, 94 (2015) 304.
5. H.L. Wu, Y.L. Cheng, L.L. Li, Z.H. Chen, H.M. Wang, Z. Zhang, *Appl. Surf. Sci.*, 253 (2007) 9387.
6. H.Y. Hsiao, H.C. Tsung, W.T. Rsai, *Surf. Coat. Technol.*, 199 (2005) 127.
7. R. Zandi-zand, A. Ershad-langroudi, A. Rahimi, *Prog. Org. Coat.*, 53 (2005) 286.
8. R.G. Hu, S. Zhang, J.F. Bu, C.J. Lin, G.L. Song, *Prog. Org. Coat.*, 73 (2012) 129.
9. L. Feng, S.H. Li, Y.S. Li, H.J. Li, L.J. Zhang, J. Zhai, Y.L. Song, B.Q. Liu, L. Jiang, D.B. Zhu, *Adv. Mater.*, 14 (2002) 1857.
10. P. Tian, Z.G. Guo, *Appl. Surf. Sci.*, 426 (2017) 1.
11. Z.X. Kang, W. Li, *J. Ind. Eng. Chem.*, 50 (2017) 50.
12. Y. Liu, J.Z. Xue, D. Luo, H.Y. Wang, X. Gong, Z.W. Han, L.Q. Ren, *J. Colloid Interface Sci.*, 491 (2017) 313.
13. L.B. Feng, Y.L. Zhu, J. Wang, X.T. Shi, *Appl. Surf. Sci.*, 422 (2017) 566.
14. J. Kuang, Z.X. Ba, Z.Z. Li, Y.Q. Jia, Z.Z. Wang, *Surf. Coat. Technol.*, 361 (2019) 75.
15. L. Liu, J.L. Lei, L.J. Li, J. Zhang, B. Shang, J.X. He, N.B. Li, F.S. Pan, *Adv. Mater. Interfaces*, 5 (2018) 1800213.
16. J. Xie, J. Hu, X.D. Lin, L. Fang, F. Wu, X.L. Liao, H.J. Luo, L.T. Shi, *Appl. Surf. Sci.*, 457 (2018) 870.
17. L.F. Chen, Z.G. Guo, *Colloid Surf. A*, 554 (2018) 253.
18. F. Guo, Q.Y. Wen, Y.B. Peng, Z.G. Guo, *J. Mater. Chem. A*, 5 (2017) 1.
19. I. You, Y.C. Seo, H. Lee, *RSC Adv.*, 4 (2014) 10330.

20. Y.F. Sheng, G.Q. Sun, T. Ngai, *Langmuir*, 32 (2016) 3122.
21. B. Shang, Y.B. Wang, B. Peng, Z.W. Deng, *J. Colloid Interface Sci.*, 482 (2016) 240.
22. Z.N. Li, C.J. Wu, K. Zhao, B. Peng, Z.W. Deng, *Colloid Surf. A*, 470 (2015) 80.
23. X.G. Zhang, Z.J. Liu, Y. Li, C.J. Wang, Y.J. Zhu, H.Y. Wang, J.T. Wang, *Chem. Eng. J.*, 371 (2019) 276.
24. W.Y. Peng, X.L. Gou, H.L. Qin, M.Y. Zhao, X.Z. Zhao, Z.G. Guo, *Chem. Eng. J.*, 352 (2018) 774.
25. Y.J. Tuo, H.F. Zhang, W.P. Chen, X.W. Liu, *Appl. Surf. Sci.*, 423 (2017) 365–374.
26. J.L. Zhang, C.D. Gu, Y.Y. Tong , W. Yan , J.P. Tu, *Adv. Mater. Interfaces*, 3 (2016) 1500694.
27. C. Lou, R. Zhang, X. Lu, C.L. Zhou, Z. Xin, *Colloid Surf. A*, 562 (2019) 8.
28. L.Y. Wang, Y.P. Yu, Q. Xiang, J. Xu, Z.X. Cheng, J.Q. Xu, *Sens. Actuators B: Chem.*, 255 (2017) 2704.
29. J.T. Wang, H.F. Wang, G.H. Geng, *Mar. Pollut. Bull.*, 127 (2018) 108.
30. L.P. Ding, J. Gao, T.S. Chung, *Sep. Purif. Technol.*, 213 (2019) 437.
31. C. Hu, W.H. Chen, T. Li, Y.X. Ding, H. Yang, S.J. Zhao, E.A. Tsiwah, X.J. Zhao, Y. Xie, *Colloid Surf. A*, 551 (2018) 65.
32. L. Zhang, D.Y. Dong, L.S. Shao, Y.F. Xia, T. Zeng, Y.H. Wang, *Colloid Surf. A*, 576 (2019) 43.
33. D. Zhang, G.L. Zheng, C. Zheng, Y.H. Wu, Z. Long, *Prog. Org. Coat.*, 134 (2019) 226.
34. Y. Li, X.G. Zhang, Y.X. Cui, H.Y. Wang, J.X. Wang, *Chem. Eng. J.*, 374 (2019) 1326.
35. Q.S. Yao, F. Zhang, L. Song, R.C. Zeng, L.Y. Cui, S.Q. Li, Z.L. Wang, E.H. Han, *J. Alloy. Compd.*, 764 (2018) 913.
36. X.K. Zhang, J. Shen, D. Hu, B. Duan, C.M. Wang, *Surf. Coat. Technol.*, 334 (2018) 90.
37. A.M. Emelyanenko, L.B. Boinovich, A.D. Modestov, A.G. Domantovsky, K.A. Emelyanenko, O.V. Dvoretskaya, *J. Electrochem. Soc.*, 163 (2016) 659.
38. J. Huang, C. Lou, D. Xu, X. Lu, Z. Xin, C.L Zhou, *Prog. Org. Coat.*, 136 (2019) 105191.
39. C.J. Lv, H.Y. Wang, Z.J. Liu, W.B. Zhang, C.J. Wang, R.F. Tao, M.L. Li, Y.J. Zhu, *Appl. Surf. Sci.*, 435 (2018) 903.
40. L.B. Boinovich, A.M. Emelyanenko, A.D. Modestov, A.G. Domantovsky, A.A. Shiryaev,K.A. Emelyanenko, O.V. Dvoretskaya, A.A. Ganne, *Corrosion Sci.*, 112 (2016) 517.
41. J. Kuang, Z.X. Ba, Z.Z. Li, Z.Z. Wang, J.H. Qiu, *Appl. Surf. Sci.*, 501 (2020) 144137.
42. W.Y. Zhao, R.J. Zhu, J.Y. Jiang, Z.M. Wang, *Appl. Surf. Sci.*, 484 (2019) 307.